Dielectric, ferroelectrics properties and impedance spectroscopy analysis of the [(Na0.535K0.480)0.966Li0.058](Nb0.90Ta0.10)O3-based lead-free ceramics

M. Saidi, Ahcène Chaouchi, Sophie d'Astorg, Mohamed Rguiti, Christian Courtois

JOURNAL OF ADVANCED DIELECTRICS
Vol. 5, No. 1 (2015) 1550007 (7 pages)

DOI: 10.1142/S2010135X15500071

World Scientific
www.worldscientific.com

Dielectric, ferroelectrics properties and impedance spectroscopy analysis of the $[(Na_{0.535}K_{0.480})_{0.966}Li_{0.058}]$ $(Nb_{0.90}Ta_{0.10})O_3$-based lead-free ceramics

M. Saidi*, A. Chaouchi*,§, S. D'Astorg†,‡, M. Rguiti†,‡ and C. Courtois†
*Laboratoire de Chimie Appliquée et Génie Chimique de l'Université Mouloud Mammeri de Tizi-Ouzou, Algérie
†Laboratoire des Matériau Céramiques et Procédés Associés — Université de Valenciennes et du Hainaut-Cambrésis Boulevard Charles de Gaull, 59600 Maubeuge, France
‡University of Lille Nord de France F-59000 Lille, France
§ahchaouchi@yahoo.fr

Received 23 December 2014; Revised 8 February 2015; Accepted 12 February 2015; Published 2 April 2015

Polycrystalline of $[(Na_{0.535}\ K_{0.480})_{0.966}\ Li_{0.058}]$ $(Nb_{0.90}Ta_{0.10})O_3$ samples were prepared using the high-temperature solid-state reaction technique. X-ray diffraction (XRD) analysis indicates the formation of a single-phase with orthorhombic structure. AC impedance plots were used as tool to analyze the electrical behavior of the sample as a function of frequency at different temperatures. The AC impedance studies revealed the presence of grain effect, from 425°C onwards. Complex impedance analysis indicated non-Debye type dielectric relaxation. The Nyquist plot showed the negative temperature coefficient of resistance (NTCR) characteristic of NKLNT. The AC conductivity results were used to correlate with the barrier hopping (CBH) model to evaluate the binding energy (W_m), the minimum hopping distance (R_{min}), the density of states at Fermi level ($N(E_f)$), and the activation energy of the compound.

Keywords: Lead-free piezo-ceramics; dielectric properties; AC impedance spectroscopy; dielectric relaxation; conductivity.

1. Introduction

Actually, $PbZr_{(1-x)}Ti_xO_3$ (PZT) and lead-based compounds constitute the best family of piezoelectric and ferroelectric materials suitable for integration in devices, such as actuators, sensors and ultrasonic transducers. However, at the present time, there are some restrictions based upon European directives and thus lead-based piezoelectric materials are only tolerated for piezoelectric devices.[1] As a consequence, new lead-free materials are the aim of studies and several recent papers[2–4] made an inventory of the compounds actually considered as potential candidates for the replacement of PZT.

Among lead-free piezoelectric systems, the niobate-based ceramics are the most promising.[5–8] For pure (Na,K) NbO_3(NKN) ceramics prepared by normal sintering, the highest piezoelectric coefficient was no more than 100 pC/N.[2] However, their piezoelectric properties could be enhanced by introducing Li and Ta, respectively, into the A and B sites of perovskite-structured NKN ceramics.[5,9–12]

On the other hand, the $[(Na_{0.535}K_{0.480})_{0.966}Li_{0.058}]$ $(Nb_{0.90}Ta_{0.10})O_3$ (NKLNT) system has been paid considerable attention on account of the existence of a orthorhombic and tetragonal morphotropic phase boundary (MPB).[13]

However, the major drawbacks of (Na,K)NbO_3-based ceramics are (i) high hygroscopicity of the used precursors, (ii) the temperature instability due to the lower orthorhombic–tetragonal transition temperature (T_{o-t}), and (iii) the difficulty to obtain fully dense ceramics due to the evaporation of potassium and sodium during the sintering process.[14–18]

For all of them, a general trend can be evidenced: (i) the evaporation of (at least) one of the alkali constituents of the MPB involves an evolution of the chemical composition and the formation of secondary phases resulting in poor properties and (ii) this mechanism is associated with abnormal gain growth, these two phenomena being probably correlated.[19,20] However, the control of the alkali content in such samples is also a key point in order to obtain suitable properties.

To address this problem, many derivatives (Na, K)NbO_3 ceramics have been developed: They are based on formation of solid solutions of NKN–$SrTiO_3$ and NKN–$LiTaO_3$, and on the use of sintering aids, e.g., $K_4CuNb_8O_{23}$, MnO_2, CuO and Bi_2O_3.[21,22] In addition, many compositions that possess different Curie temperatures, a broad range of electrical properties and with their own MPB, can be produced by changing the ratio of Li to Ta or Sb within the NKN systems. Particularly, the textured (Li, Ta, Sb)-modified NKN

ceramics exhibit piezoelectric properties comparable to those of a hard PZT.[23]

In addition, it is well known that defects such as A-site vacancies, space charge electrons or oxygen vacancies have great influence on ferroelectric fatigue or ionic conductivity of the material.[24–26] The defects play also a decisive role in different applications, it is very important to gain a fundamental understanding of their conductivity mechanisms of materials. Various kinds of defects are always suggested as being responsible for the dielectric relaxations at high temperature range. The AC impedance analysis is a powerful mean to distinguish effects between the grain boundary, the grain and the electrodes, which are usually the traps for defects. It is also useful to establish its relaxation mechanism by appropriately assigning different values of resistance and capacitance to the grains and grain boundaries effects.

In this paper, we focused our research on the NKLNT composition, which exhibits quite good properties with excellent piezoelectric characteristics.[13] The aim of this work was first to study the dielectrics, ferroelectric and piezoelectric properties. Then a detailed analysis by AC impedance spectroscopy was carried out to characterize the dielectric relaxation. The AC conductivity data were used to estimate the apparent activation energy, the density of states at Fermi level, and the minimum hopping length.

2. Experimental Procedure

The NKNLT compound was prepared by solid-state reaction using reagent grades powders of Na_2CO_3, K_2CO_3, Li_2CO_3, Nb_2O_5 and Ta_2O_5 (purity $> 99\%$). These compounds were stoichiometrically mixed using isopropanol and zircon balls in a Teflon jar for 2 h. The slurry was subsequently dried. The obtained mixture was manually reground and heat treated at 850°C for 2 h in air. The powder was finally reground using the same process than before in ethanol solution for 2 h.

To manufacture pellets, an organic binder (Polyvinyl alcohol, 5 wt.%) was manually added to the powder and disks (7 and 13 mm in diameter, 1 and 1.5 mm thickness, respectively) were shaped by uni-axial pressing under 100 MPa. The green samples were finally sintered in air at 1100°C for 2 h, with heating and cooling rates of 150°C/h. The crystallized phase composition has been identified by X-ray diffraction (XRD) technique using the Cu kα X-ray radiation (Philips X'Pert) and the microstructures were observed using a Scanning Electron Microscopy (SEM Philips XL'30). The specimens were polished and electroded with a silver paste. The dielectric and electric properties were determined using HP4284A meter versus temperature (from 20°C to 500°C), and the frequency range from 100 Hz to 1 MHz. For piezoelectric measurements, the polarization of the samples occurred at room temperature under different poling. The piezoelectric coefficient (d_{33}) was measured using a piezoelectric d_{33} meter (Piezotest PM 200) at a frequency of 100 Hz. *P–E* hysteresis loops were obtained using Radiant Precision Workstation ferroelectric testing system.

3. Results and Discussion

3.1. *Phase analysis and microstructure*

Figure 1 shows the XRD patterns of NKNLT sintered samples. The pattern reveals a single perovskite structure without any secondary phases, suggesting that homogeneous solid solutions of NKNLT are formed. The NKNLT system exhibits an orthorhombic structure which has been indexed according to the data of Kumada *et al.* ($KNbO_3$ with lattice constants: $a = 3.976$ Å, $b = 5.695$ Å and $c = 5.717$ Å with space group *Amm*2).[27] The unit cell parameters for the NKNLT composition were determined by fitting the XRD patterns of the samples. The obtained lattice parameters are: $a = 4.0009$ Å, $b = 5.7075$ Å and $c = 5.7075$ Å. The slight variation of lattice parameters is due to the formation of NKNLT solid solution. In this solid solution, Na^+, K^+ and Li^+ should occupy A^+ sites, while Nb^{5+} and Ta^{5+} should occupy B^{5+} sites due to their valence and ionic radii.

Figure 2 shows SEM micrographs of sintered ceramic sample. It shows a quasi-cubic morphology with clear grain boundaries. It can also be seen that the ceramics with

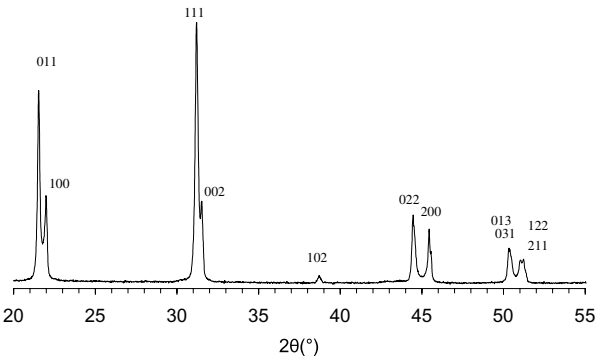

Fig. 1. XRD patterns of NKNLT composition sintered at 1100°C for 2 h.

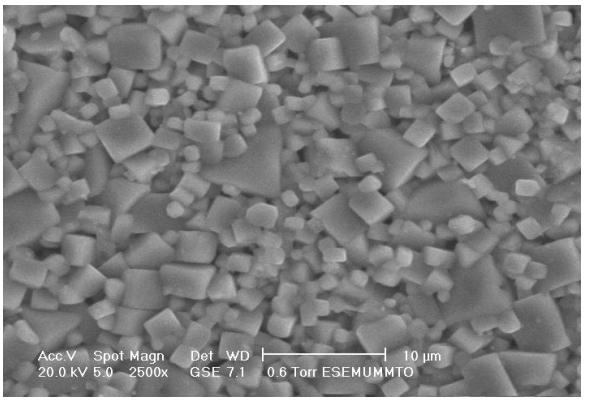

Fig. 2. SEM of fracture for the sintered ceramic.

relatively homogenous microstructure and low porosity can be obtained, the average grain size being about 1 to 4 μm.

3.2. *Dielectric and ferroelectric studies*

Figure 3 shows the temperature dependence of the dielectric constant (ε_r) and dielectric losses tangent (tan δ) of NKNLT ceramics at the frequencies of 1, 10 and 100 kHz, respectively.

There are two anomalisms at the measured temperature range from room temperature to 400°C. These anomalisms are considered to correspond to the following phase transitions from: the transition orthorhombic phase to tetragonal phase at lower temperature (O–T), and the transition from tetragonal phase to cubic phase at higher temperature (T_C). The obtained dielectric loss (tan δ) was lower, and the dielectric constant (ε_r) varied from 800 to 7000 at room temperature and at T_C, respectively. The dielectric loss increases rapidly at higher temperature due to the rapid increase of conductivity of the materiel.

Figure 4 shows the *P–E* hysteresis loops of the NKNLT ceramics. It shows a well-saturated *P–E* hysteresis loop, suggesting that the ceramic exhibits a good ferroelectric property. The obtained coercive field E_C and remanent polarizations P_r are 2.5 kV/mm and 36.25 μC·cm^{-2}, respectively.

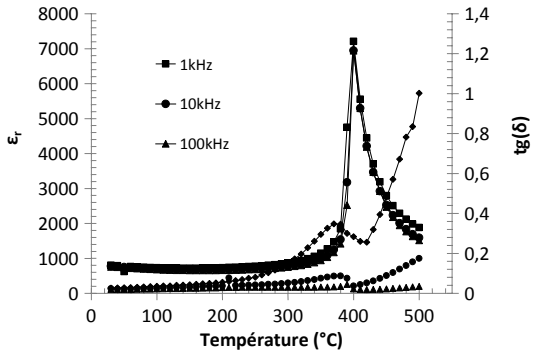

Fig. 3. Temperature dependence of permittivity and dielectric loss at different frequencies of NKNLT.

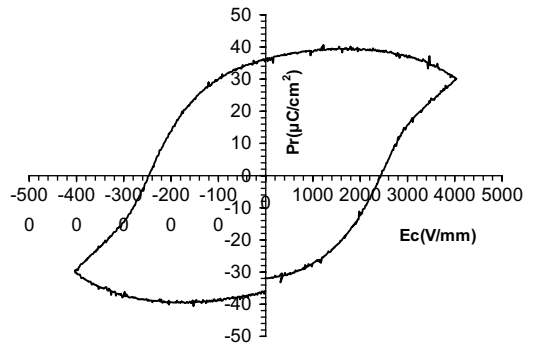

Fig. 4. *P–E* hysteresis loops of the NKNLT ceramics.

3.3. *Complex impedance spectrum analysis*

The complex impedance spectroscopic (CIS) technique is used to analyze the electrical response of polycrystalline samples in a wide range of frequencies and temperatures. This technique is based on the application of an alternating voltage signal to a sample and the measurement of the corresponding phase shifted current response. The complex impedance spectroscopy is a powerful tool to analyze the microstructure and properties relationship of the material. The physical process occurring inside the sample can be modeled as an equivalent circuit using impedance spectra. The electrical AC response of the material may be represented in any of the four basic formalisms via complex permittivity (ε^*), complex impedance (Z^*), complex admittance (Y^*) and complex electric modulus (M^*), which are interrelated to each other.[28] These relations offer a wide scope for a graphical analysis of the various electrical parameters under different experimental conditions (temperature and frequency). From the microstructural point of view, a ceramic sample is composed of grains and grain boundaries, exhibiting different resistivity (ρ) and dielectric permittivity (ε). The real part (Z') and the imaginary part (Z'') of the complex impedance are given by the following equations[29]:

$$Z' = R_g/(1 + (\omega R_g C_g)^2) + R_{gb}/(1 + (\omega R_{\rm gb} C_{\rm gb})^2), \quad (1)$$

$$Z'' = \omega R_g^2 C_g/(1 + (\omega R_g C_g)^2) + \omega R_{\rm gb}^2 C_{\rm gb}/(1 + (\omega R_{\rm gb} C_{\rm gb})^2), \quad (2)$$

where R_g and C_g are the resistance and capacitance of the grain, while $R_{\rm gb}$ and $C_{\rm gb}$ are the resistance and capacitance of the grain boundary, respectively.

Figure 5 shows the variation of the real part of impedance (Z') with frequency at different temperatures. It is observed that the magnitude of Z' decreases with increasing the frequency and temperature, indicating an increase in ac conductivity with increase in temperature and frequency. The Z' values for all temperatures merge at high frequency (> 10 kHz). This may be attributed to the increase of ac conductivity with temperature and frequency in the higher

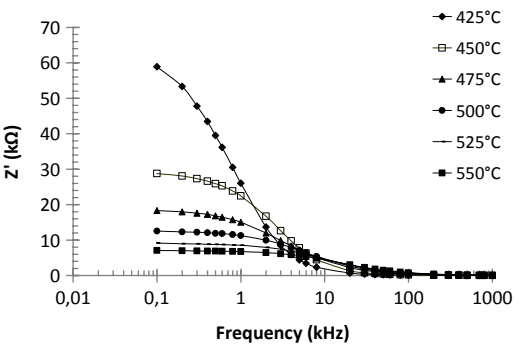

Fig. 5. Variation of real part of impedance (Z') of NKNLT with frequency at different temperatures.

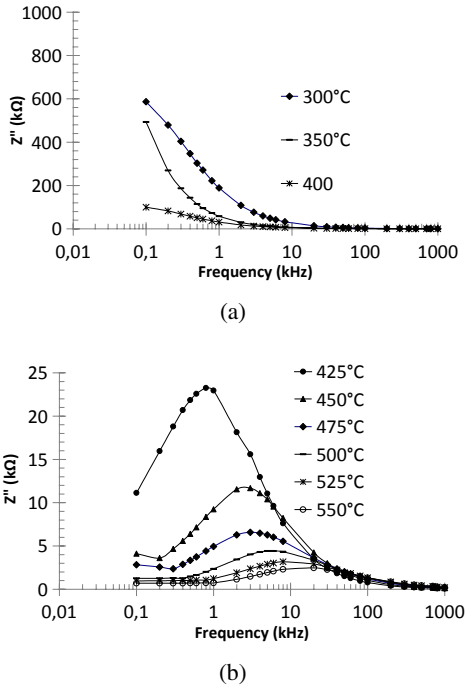

Fig. 6. Variation of imaginary part (Z'') of impedance with frequency at different temperatures.

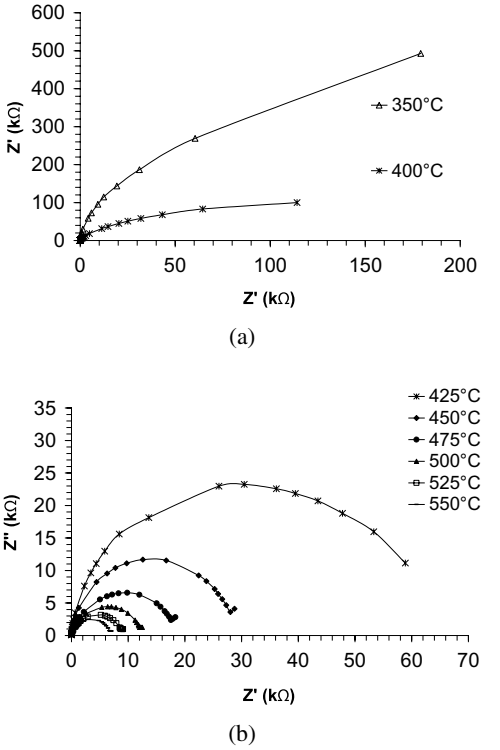

Fig. 7. Complex impedance plots (Z'' versus Z') of NKNLT at different temperatures.

frequency region due to the removal of space charge as a result of reduction in potential barrier height.[30] Furthermore, at low frequency, Z' values decrease with an increase in temperature and reveal negative temperature coefficient of resistance (NTCR) behavior similar to that of semiconductors.

Figures 6(a) and 6(b) show the variation of imaginary part (Z'') with frequency and temperature. As the temperature increases, the obtained peaks are more and more flattened in this specimen indicating relaxation is stronger at higher temperatures (Fig. 6(b)). It can be seen that the curves display broad and low intensity peaks with asymmetrical shape. The broadening of the peak and half-widths of the peaks indicate multiple relaxations and deviations from Debye behavior.[31]

In order to study the impedance spectrum corresponding to different effects such as grain boundaries, grains (bulk or intrinsic properties of material) and electrode contribution, Cole–Cole analysis[32] has been performed.

Figures 7(a) and 7(b) show Cole–Cole plots (Z'' versus Z') at various temperatures. For temperature measurements below 400°C, there is no semicircle formation (Fig. 7(a)). By increasing temperature, the Z'' versus Z' curve changes and semicircles appear indicating an increase of the materials conductivity (Fig. 7(b)).

The presence of a single semicircular arc passing through the origin in the entire frequency region for all the temperatures indicates that the relaxation mechanism in NKNLT may be only a grain effect. Hence it is appropriate to fit the Z-plot to a single R_gC_g parallel circuit due to the fact that the response peaks of the grain boundaries are not present. The expression for Z^* is given by:

$$Z^* = Z' + iZ'' = R_g/(1 + i\omega R_g C_g), \tag{3}$$

where R_g and C_g are the grain resistance and grain capacitance, respectively. Unfortunately, Eq. (3) cannot be used to describe the experimental data very well due to the depressed nature of the semicircular arcs. Furthermore, for Debye type relaxation, one expects semicircular plots with the center located on the Z'-axis, whereas for a non-Debye type relaxation these Argand plane plots are close to semicircular arcs with end points on the real axis and the center lies below this axis. The complex impedance in such a case can be described as[33]:

$$Z^*(\omega) = Z' + iZ'' = R/(1 + (i\omega/\omega_0)^{1-\alpha}, \tag{4}$$

where α represents the magnitude of the departure of the electrical response from an ideal condition and this can be determined from the location of the center of the semicircles. Further, it is known that when α approaches to zero, i.e., $\{(1-\alpha) = 1\}$, Eq. (4) gives rise to classical Debye's formalism. It can be seen from the impedance plots (Fig. 7(b)) that the curves are not full semicircle, they are depressed one, i.e., center of semicircles lie little below the abscissa (Z') axis ($\alpha > 0$), which increases with the rise in temperature suggesting the dielectric relaxation to be non-Debye type in NKNLT composition.

3.4. *Conductivity studies*

The ac conductivity was obtained according to the equation $\sigma_{ac} = Z'^2 t/(Z'^2 + Z''^2)A$, where t and A are the thickness and area of the electrode, respectively. Figure 8 shows the plot of AC conductivity versus frequency at different temperatures. The frequency dependence of the material conductivity exhibits both low and high frequency dispersion phenomena. But it can be observed that the dispersion is more important at low frequency, the AC conductivity of the materials obeys the Jonscher's power law equation[34] given by:

$$\sigma_{(\omega)} = \sigma_{dc} + A\omega^n, \tag{5}$$

where n is the frequency exponent in the range of $0 < n < 1$, A and n are thermally activated quantities, hence electrical conduction is thermally activated process.

The origin of the frequency dependence of conductivity lies to the relaxation phenomena arising due to mobile charge carriers. When the mobile charge carriers hops to a new site from its original position, it remains in a state of displacement between two potential energy minima, which includes contributions from other mobile defects. After a sufficiently long time, the defect could relax until the two minima in lattice potential energy coincide with the lattice site.

The values of exponent n, σ_{dc} and A were obtained by fitting Eq. (5) (σ_{ac} versus ω) from 10^3 to 10^5 Hz at different temperatures. The fit quality is usually evaluated by comparing the squared coefficient of linear correlation coefficient (R^2) obtained for each temperature (see Table 1). It can be seen that the value of n is always less than 1 and decreases when temperature increases. The model based on hopping of charge carriers over potential barrier,[35] predicts a decrease of the (n) index with the increase in temperature and hence this is consistent with the experimental results. Therefore, the conduction in the system may be considered to be due to the short-range translational type hopping of charge carriers. This indicates that the conduction process is a thermally activated process.

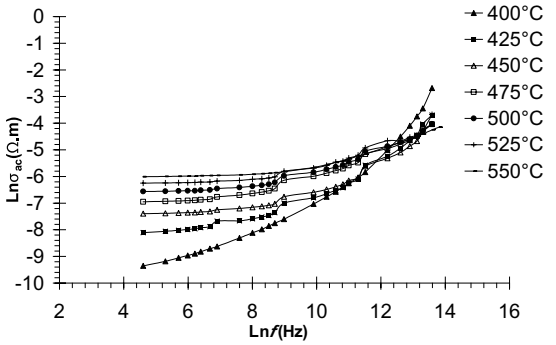

Fig. 8. Frequency dependence of σ_{ac} conductivity at different temperatures.

Table 1. The fitting parameters obtained from experimental data of the conductivity as function of frequency (σ_{ac} versus ω) using the Jonscher' power law.

Temperature (°C)	σ_{dc} $(\Omega/cm)^{-1}$	A	n	R^2
400	$1.5{\cdot}10^{-6}$	$1.7551{\cdot}10^{-7}$	0.83785	0.9994
425	$3.4{\cdot}10^{-6}$	$3.5326{\cdot}10^{-7}$	0.74597	0.99965
450	$6{\cdot}10^{-6}$	$4.8851{\cdot}10^{-7}$	0.71222	0.99993
475	$7.7{\cdot}10^{-6}$	$5.1239{\cdot}10^{-6}$	0.56429	0.99984
500	$9.7{\cdot}10^{-6}$	$7.5199{\cdot}10^{-6}$	0.53894	0.99986

Hopping conduction mechanism is generally consistent with the existence of a high density of states in the materials having bandgap similar to that semiconductor.

Using correlated barrier hopping (CBH) model,[36] the binding energy has been calculated according to the following equation:

$$\beta = \frac{6k_B T}{w_m}, \tag{6}$$

where $\beta = 1 - n$ and w_m is the binding energy, which is defined as energy required to remove an electron completely from one site to another site. The obtained w_m values decrease in slope when temperature increases. It is due to the decrease in binding energy of the material as illustrated in Fig. 9.

Using the values of the binding energy, minimum hopping distance R_{min} is calculated thanks to Eq. (7)[37]:

$$R_{min} = \frac{2e^2}{\pi\varepsilon\varepsilon_0 W_m}, \tag{7}$$

where ε_o is the permittivity of free space and ε is the dielectric constant of the material. The variation of R_{min} with temperature is shown in Fig. 9. It is observed that the R_{min} values increases with increasing temperature. It can be supposed that the charge transport takes place through the infinite percolation path at lower frequency region. The charge transport mechanism is dominated by hopping into finite clusters at higher frequency region.

The AC conductivity data have been used to evaluate the density of states at Fermi level $N(E_f)$ using the following equation[38]:

$$\sigma_{ac}(\omega) = (\pi/3)e^2\omega k_B T\{(N(E_f)\}^2\alpha^{-5}\{\ln(f_0/\omega)\}^2, \tag{8}$$

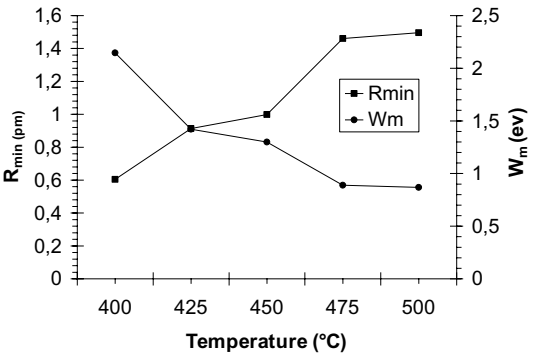

Fig. 9. Temperature dependence of W_m and R_{min} of NKLNT obtained at 1 kHz.

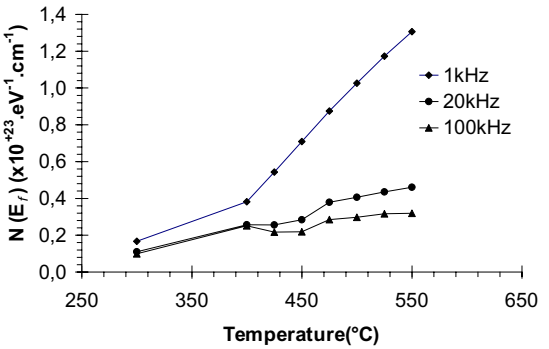

Fig. 10. Variation of density of state at Fermi level of NKLNT ceramic with temperature.

where e is the electronic charge, f_o the photon frequency, and α is the localized wave function, assuming $f_o = 10^{13}$ Hz, $\alpha = 10^{10}\,\mathrm{m}^{-1}$.

Figure 10 illustrates the variation of $N(E_f)$ with temperature at different frequencies. It is observed that the value of $N(E_f)$ increases with temperature. The high $N(E_f)$ values suggest that the hopping between the pairs of sites dominates the mechanism of charge transport.[39]

The electronic thermal conductivity accounts for the total thermal conductivity are given by[40]:

$$k = L\sigma_{ac}T[1 + (3/4\pi^2)\{(E_a/k_BT) + 4\}^2], \qquad (9)$$

where L is the Lorentz number. The thermal conductivity of grain increases with increasing temperature and it exhibits reasonably low thermal conductivity (Fig. 11).

The dc conductivity, σ_{dc}, of the sample has been evaluated from the impedance spectrum using the relation $\sigma_{dc} = t/AR_b$ where R_b is the bulk resistance (obtained from the intercept of the semicircular arcs (Z'') on the real axis (Z')), t the thickness, and A the surface area of the sample. Figure 12 shows the variation of ln σ_{dc} with $10^3/T$. It is observed that σ_{dc} increases with temperature confirming again the NTCR behavior. The nature of variation is linear and follows the Arrhenius relationship given by:

$$\sigma_{dc} = \sigma_0 \exp(E_{a1}/k_BT), \qquad (10)$$

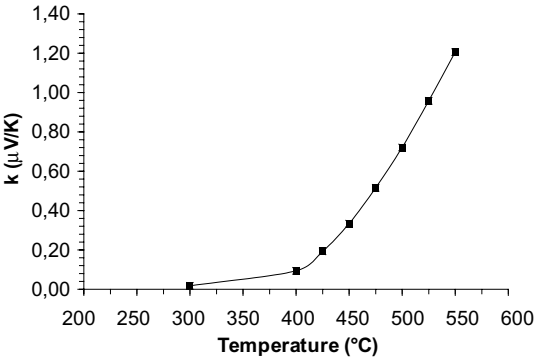

Fig. 11. The electronic thermal conductivity accounts.

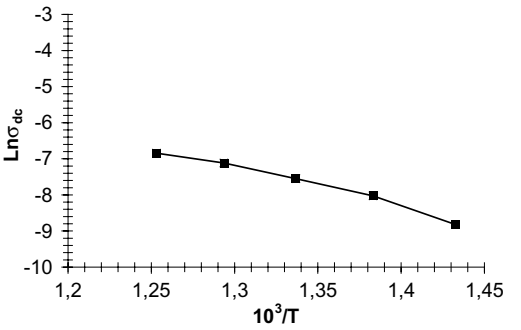

Fig. 12. The variation of ln σ_{dc} with $10^3/T$.

where E_{a1} is the activation energy of conduction and T is the absolute temperature. The value of activation energy (E_{a1}) calculated from the slope of ln σ_{dc} with $10^3/T$ curve is found to be 0.94 eV. Such a value of activation energy indicates that the conduction mechanism of studied system may be due to the polaron hopping based on electron carriers. Such a value of activation energy was found for $Ba(Zn_{1/2}W_{1/2})O_3$ perovskite.[28]

Figure 13 shows the relaxation variation time (ln τ) with inverse of absolute temperature ($10^3/T$). The characteristic of the relaxation time (τ) was calculated from Z'' versus frequency plots using the relation: $\tau = 1/\omega = 1/2\pi f_{max}$, where f_{max} is the relaxation frequency at which z'' was found to be maximum.

The data are described by Arrhenius' expression:

$$\tau = \tau_0 \exp(E_{a2}/k_BT), \qquad (11)$$

where E_{a2} is the activation energy for the conduction relaxation derived from $Z''(f)$ functions, where τ_0 is the pre-exponential factor or characteristic relaxation time constants, respectively. The value of activation energy (E_{a1}) as calculated from the slope of ln τ with $10^3/T$ curve is found to be 1.04 eV.

The E_{a1} and E_{a2} calculated activation energies are relatively close to each other in the studied temperature range. It corresponds to the required energy for oxygen vacancies motion (1 eV).[41] This confirms that the observed conductivity is due to the movements of oxygen vacancies in the material. Its phenomena can also be explained by the volatility of

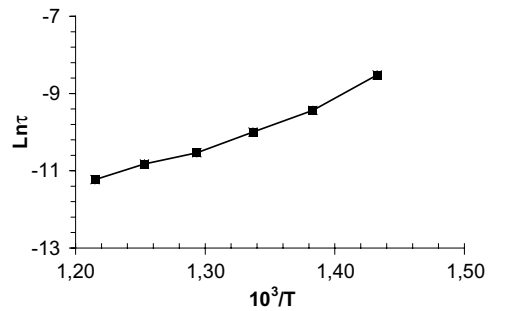

Fig. 13. Arrhenius diagram of relaxation times Ln(τ) as a function of reciprocal temperature (1/T).

alkaline element (K and Na) at high temperature during sintering, involving the formation of oxygen vacancy, which can be noted by the Kroger–Vink notation as:

$$[(Na_{0.535}K_{0.480})_{0.966}Li_{0.058}](Nb_{0.90}Ta_{0.10})O_3 \times \frac{\text{At high temperature}}{\text{During sintering}} [(Na^{+}_{0.535}K^{+}_{0.480})_{0.966-x}(\mathbf{v'_{Na}\ or\ v'_{K}})_x Li^{+}_{0.058}] \times (Nb^{+5}_{0.90}Ta^{+5}_{0.10})O^{-2}_{3-x/2}(\mathbf{v''_o})_{x/2} + x/2(\overrightarrow{Na_2O}) \text{ or } x/2(\overrightarrow{K_2O})$$

where Na^+- or K^+-site vacancies in the structure are v'_{Na} and v'_K, respectively, v'_O being the oxygen-ion vacancy.

4. Conclusions

Polycrystalline NKLNT perovskite, prepared through a high-temperature solid-state reaction technique, was found to be a single-phased perovskite-type. Impedance analyses indicated the presence of grain effect in NKNLT ceramics. The dielectric relaxation was found to be of non-Debye type and the relaxation frequency shifted to higher values with the increase of temperature.

The ac conductivity is found to follow the universal power law, which can be explained by the CBH model.

The activation energy (E_a) of the compound under investigation has been calculated using the Arrhenius expression (derived from $Z''(f)$ and σ_{dc}). The value of activation energy (E_a) as calculated from the slope is found to near 1 eV, this value is due to the movements of oxygen vacancy in the material.

References

[1]Directive 2002/95/EC, On the restriction of the use of certain hazardous substances in electrical and electronic equipment, Official Journal of the European Union, 13 February 2003.
[2]M. D. Maeder, M. D. Damjanovic and N. Setter, Lead free piezoelectric materials, *J. Electroceram.* **13**, 385 (2004).
[3]J. Rodel, A. B. N. Kounga, M. Weissenberger-Eibl, D. Koch, A. Bierwisch, W. Rossner, M. J. Hoffmann, R. Danzer and G. Schneider, Development of a roadmap for advanced ceramics, 2010–2025, *J. Eur. Ceram. Soc.* **29**, 1549 (2009).
[4]J. Rodel, W. Jo, K. T. P. Seifert, E. Anton, T. Granzow and D. Damjanovic, Perspective on development lead-free piezoceramics, *J. Am. Ceram. Soc.* **92**, 1153 (2009).
[5]Y. Saito, H. Takao, T. Tani, T. Nonoyama, K. Takatori, T. Homma, T. Nagaya and M. Nakamura, *Nature (Lond.)* **432**, 84 (2004).
[6]Y. Y. Wang, J. G. Wu and D. Q. Xiao, *J. Alloys Compd.* **459**, 414 (2008).
[7]K. Wang, J. F. Li and N. Liu, *Appl. Phys. Lett.* **93**, 092904 (2008).
[8]J. G. Wu, D. Q. Xiao and Y. Y. Wang, *Scr. Mater.* **59**, 750 (2008).
[9]Y. Wang, J. Wu, D. Xiao, J. Zhu, P. Yu, L. Wu and X. Li, *J. Alloys Compd.* **462**, 310 (2008).
[10]P. Zhao, B. P. Zhang and J. F. Li, *Scr. Mater.* **58**, 429 (2008).
[11]J. G. Wu, D. Q. Xiao and Y. Y. Wang, *J. Appl. Phys.* **103**, 024102 (2008).
[12]R. Zuo, D. Lv, J. Fu, Y. Liu and L. Li, *J. Alloys Compd.* **9**, 123 (2008).
[13]P. Zhao, B.-P. Zhang and J.-F. Li, *Scr. Mater.* **58**, 429 (2008).
[14]R. E. Jaeger and L. Egerton, *J. Am. Ceram. Soc.* **45**, 209 (1962).
[15]L. Egerton and D. M. Dillom, *J. Am. Ceram. Soc.* **42**, 438 (1959).
[16]Z. S. Ahn and W. A. Schulze, *J. Am. Ceram. Soc.* **70**, 18 (1987).
[17]J. H. Yoo, D. H. Kim, Y. H. Lee, I. H. Lee, S. H. Lee, I. S. Kim *et al.*, *Integr. Ferroelectr.* **105**, 18 (2009).
[18]D. Gao, K. W. Kwok, D. Lin and H. L. W. Chan, *J. Mater. Sci.* **44**, 2466 (2009).
[19]Y. Wang, D. Damjanovic, N. Klein, E. Hollenstein and N. Setter, Compositional inhomogeneity in Li- and Ta-modified (K,Na) NbO_3 ceramics, *J. Am. Ceram. Soc.* **90**, 3485 (2007).
[20]Y. Wang, D. Damjanovic, N. Klein, E. Hollenstein and N. Setter, High-temperature instability of Li- and Ta-modified (K,Na)NbO_3 piezoceramics, *J. Am. Ceram. Soc.* **91**, 1962 (2008).
[21]Y. Lee, B. Seo, Y. Oh, J. Yoo, I. Kim and J. Song, *J. Kor. Phys. Soc.* **57**, 959 (2010).
[22]Y. Saito, H. Takao, I. Tani, T. Nonoyama, K. Takatori, T. Homma, T. Nagaya and M. Nakamura, *Nature* **432**, 84 (2004).
[23]L. Wu, D. Xiao, J. Wu, Y. Sun, D. Lin, J. Zhu *et al.*, *J. Eur. Ceram. Soc.* **28**, 2963 (2008).
[24]K. Goda and M. Kuwabara, *Ceram. Trans.* **22**, 503 (1991).
[25]O. Bidault, P. Goux, M. Kchikech, M. Belkaoumi and M. Maglione, *Phys. Rev. B* **49**, 7868 (1994).
[26]W. Li, A. P. Chen, X. U. Lu and J. S. Zhu, *J. Appl. Phys.* **98**, 024109 (2005).
[27]N. Kumada, T. Kyoda, Y. Yonesaki, T. Takei and N. Kinomura, Preparation of $KNbO_3$ by hydrothermal reaction, *Mater. Res. Bull.* **42**, 1856 (2007).
[28]I. M. Hodge, M. D. Ingram and A. R. West, Impedance and modulus spectroscopy of polycrystalline solid electrolytes, *J. Electroanal. Chem.* **74**, 125 (1976).
[29]J. R. Macdonald, *Impedance Spectroscopy* (Wiley, New York, 1987).
[30]K. Lily, K. Kumari, K. Prasad and R. N. P. Choudhary, *J. Alloys Compd.* **453**, 325 (2008).
[31]Y. M. Li, R. H. Liao, X. P. Jiang and Y. P. Zhang, *J. Alloys Compd.* **484**, 961 (2009).
[32]K. S. Cole and R. H. Cole, *J. Chem. Phys.* **9**, 341 (1941).
[33]J. Liu, C. Duan, W. N. Mei, R. W. Smith and J. R. Hardy, *J. Appl. Phys.* **98**, 093703 (2005).
[34]A. K. Jonscher, *Nature* **267**, 673 (1977).
[35]S. R. Eilliot, *Philos. Mag. B* **37**, 553 (1978).
[36]S. Mollah, K. K. Som, K. Bose and B. K. Chaudri, *J. Appl. Phys.* **74**, 931 (1993).
[37]R. Salam, *Phys. Status Solidi A* **117**, 535 (1990).
[38]G. D. Sharma, M. Roy and M. S. Roy, *Mater. Sci. Eng. B* **104**, 15 (2003).
[39]K. Lily, K. Kumari, K. Prasad and K. L. Yadav, *J. Mater. Sci.* **42**, 6252 (2007).
[40]E. Abd El-Wahabb, *Vacuum* **57**, 339 (2000).
[41]S. Sen, R. N. P. Choudhary and P. Pramanik, *Physica B* **387**, 56 (2007).